Theoretical Predictions of Energetic Molecular Crystals at Ambient and Hydrostatic Compression Conditions Using Dispersion Corrections to Conventional Density Functionals (DFT-D)

Dan C. Sorescu*,† and Betsy M. Rice‡

U.S. Department of Energy, National Energy Technology Laboratory, Pittsburgh, Pennsylvania 15236 and U.S. Army Research Laboratory, Aberdeen Proving Ground, Maryland 21005

Received: January 14, 2010; Revised Manuscript Received: February 23, 2010

Theoretical predictions of the crystallographic properties of a series of 10 energetic molecular crystals have been done using a semiempirical correction to account for the van der Waals interactions in conventional density functional theory (termed DFT-D) as implemented in a pseudopotential plane-wave code. This series contains compounds representative for energetic materials applications, that is, hexahydro-1,3,5-trinitro-1,3,5-*s* triazine (α- and γ-RDX phases), 1,3,5,7-tetranitro-1,3,5,7-tetraaza-cyclooctane (β-, α-, and δ-HMX phases), 2,4,6,8,10,12-hexanitrohexaazaisowurtzitane (CL20) (ε-, β-, and γ-HNIW phases), nitromethane (NM), trans-1,2,-dinitrocyclopropane, 1,2,3,5,7-pentanitrocubane (PNC), pentaerythritol tetranitrate (PETN), 2,4,6-trinitro-1,3,5-benzenetriamine (TATB), 2,4,6-trinitrotoluene (TNT-I phase), and 1,1-diamino-2,2-dinitroethylene (FOX-7), systems belonging to diverse chemical classes that encompass nitramines, nitroalkanes, nitroaromatics, nitrocubanes, nitrate esters, and amino-nitro derivatives. At ambient pressure, we show that the DFT-D method is capable of providing an accurate description of the crystallographic lattice parameters with error bars significantly lower than those obtained using conventional DFT. Practically, for all crystals considered in this study the predicted lattice parameters are within 2% from the corresponding experimental data [α-RDX (1.58%), β-HMX (0.64%), ε-HNIW (1.42%), NM (0.75%), DNCP (1.99%), TATB (1.74%), TNT-I (0.92%), PNC(0.78%), PETN(1.35%), FOX-7(1.57%)], with the best level of agreement being found for systems where experimental data have been collected at low temperatures. A similar good agreement of the predicted and experimental crystallographic parameters was obtained under hydrostatic compression conditions as demonstrated for the cases of RDX, HMX, CL20, NM, TATB, and PETN crystals. These results indicate that the DFT-D method provides significant improvements for description of intermolecular interactions in molecular crystals at both ambient and high pressures relative to conventional DFT. In this last case, large errors of the predicted lattice parameters have been found at low pressures; theoretical values approach the experimental results only at pressures in excess of 6 GPa.

I. Introduction

The possibility to predict the crystallographic structure and mass density of molecular energetic materials is one of the essential tools in contemporary research in the quest for discovery of new ingredients to be used in advanced energetic formulations. The need for such capabilities is motivated by the fact that estimates of performances of these materials such as the detonation pressures and velocities require knowledge of the material density.[1–3]

The task to determine the packing of molecular crystals starting from the structural analysis of the composing molecules and of the interactions among them continues to represent a significant challenge.[4] The main issue is the understanding of the determining factors that ultimately govern the molecular packing, specifically the interplay between thermodynamics and kinetics and the ability to control the polymorphism. The importance of such problems expands beyond the field of energetic materials; several other chemical areas including catalysis, pharmaceutical, or separations industries can benefit from advances in crystal structure prediction.

One of the methods largely used for crystal structure prediction is based on minimization of the lattice energy using a given set of force fields to describe the intermolecular and in some instances the intramolecular interactions between molecules.[5] In this case, a large set of initial structures selected either randomly or systematically are considered as initial candidates for energy minimization. After crystal packing energy minimization, the final structures are ranked according to their likelihood of formation. This general approach has had only partial success in the past as demonstrated by a series of blind tests organized by Cambridge Crystallographic Data Centre.[6–8] One of the major problems identified early in these tests[6] is the relatively large number of structures with total energies within few kilojoules per mole of the global minimum. Such a close energetic separation leads to difficulties in identification of the most favorable candidates without correlation to experimental data. Different solutions for further progress have been proposed in order to solve such limitations. Among these were improvements in force fields that could describe simultaneously conformational changes and packing energies[8] and for including entropic contributions to free energy.[9] Despite the significant efforts of a large number of groups to identify the optimal computational methods for crystal structure prediction[6–8] only recently, at the completion of the fourth blind test, significant

* To whom correspondence should be addressed.
† National Energy Technology Laboratory.
‡ The U.S. Army Research Laboratory.

10.1021/jp100379a
Published on Web 03/12/2010

progress in this area has been announced.[10] The best results in this case were obtained by Neumann, Leusen, and Kendrick who were able to predict the crystal structures of four target systems based on the use of a dispersion corrected density functional theory method.[11]

In the area of energetic materials, much of the early effort has been dedicated to development of the group additivity methods for solid state density prediction[3,12] or for development of ab initio crystal structure prediction methods using classical force fields.[13] In this context, our own work has focused on development and assessment of the interaction potentials capable of describing accurately both the molecular packing and the dynamic processes in energetic materials.[14–21] The essence of these models consists in the development of simple Buckingham (exp-6) intermolecular potentials plus Coulombic interactions obtained through fitting atom-centered partial charges to a quantum-mechanically determined electrostatic potential. These models originally fitted to describe the intermolecular interactions only for the case of RDX (1,3,5-hexahydro-1,3,5,-s-triazine) crystal[14] were proven to be transferable to a wide variety of CHNO crystals with functional groups common to energetic materials. This database of compounds used to demonstrate transferability across chemical classes included initially 30 different nitramines[14–18] and 51 other molecular compounds (nitroalkanes, nitroaromatics, nitrocubanes, polynitroadamantanes, polynitropolycycloundecanes, polynitropolycylo-dodecanes, hydoxy-nitro derivatives, nitrobenzonitriles, nitrobenzotriazoles, and nitrate esters).[19–21] Subsequently, transferability of these potential parameters across classes of energetic crystals has been demonstrated using both molecular packing and molecular dynamic simulations performed at different temperatures and pressures conditions. An even more rigorous test of these force fields was obtained through subjection of a set of 174 CHNO crystals to ab initio crystal structure prediction methods.[22] An overarching conclusion of all these studies is that accurate prediction of the crystallographic structure of energetic molecular crystals can be obtained only if an adequate description of the intermolecular interactions, including dispersion interactions, is considered.

The lack of an accurate description of the dispersion interactions is prone to lead to highly inaccurate values for intermolecular interactions in molecular crystals due to underestimation of the attractive forces between molecules resulting in a corresponding overestimation of the intermolecular distances. This has been manifested in results obtained using conventional density functional theory (DFT) as applied to energetic molecular crystals.[23] In this study, Byrd et al.[23] have obtained large deviations in the predicted lattice parameters of a series of energetic materials at ambient pressure, with errors as high as 9.6% relative to experimental values. A subsequent study by Byrd and Rice showed that an increase in pressure diminishes the importance of the dispersion interactions relative to the increasing contribution of the repulsive interactions.[24] As a result, the inaccuracies of the predicted intermolecular distances and lattice parameters relative to experimental data were found to decrease but only for pressures larger than 6−7 GPa.[24] These results point to the fact that conventional DFT method cannot provide reliable results for intermolecular interactions in systems for which van der Waals (vdW) interactions are the major component.

Development of DFT methods capable of describing soft matter and vdW complexes represents an active area of current interest. Several different types of methods have been proposed in recent years to handle the dispersion interactions. These range from modifications of the exchange-correlation functionals to describe nonlocal dispersion interactions,[25,26] to dispersion-corrected atom-centered potentials (DCACPs)[27,28] and dispersion-corrected DFT (DFT-D)[29] methods.

In this paper, we have used the DFT-D method for description of the intermolecular interactions. In this case a semiempirical correction term proportional to C_6R^{-6} is added to Kohn−Sham energy functional, where the C_6 parameter is proportional to atomic polarizabilities and first ionization energies and R is the interatomic distance. This term is further modified by a damping function that attenuates this interaction term at short interatomic distances to avoid electron correlation double-counting effects and avoid near-singularities at small R.[29] The performances of the DFT-D method have been tested for a variety of systems including graphene sheets,[30,31] simple layered hydroxides and clays,[32] graphite, and molecular crystals.[31] In the current research effort, we extend our previous studies based on the use of classical force fields to predict the non reactive physical properties of energetic molecular crystals using the DFT-D method. For this purpose we assess the performances of the DFT-D method for a representative series of energetic material compounds at both ambient and under hydrostatic compression conditions. As discussed above the conventional DFT methods fails to predict accurately the crystallographic properties at these conditions.

The organization of the paper is as follows. In Section 2 we discuss briefly the essential aspects of the DFT-D method and provide specific details of the computational parameters used in calculations. The results of the predicted parameters for a set of 10 molecular crystals at both ambient pressure and under compression are analyzed in Section 3 together with corresponding experimental data and results from other theoretical studies. The main conclusions of this work are summarized in Section 4.

2. Computational Method

The PWscf program,[31] which is part of the Quantum-ESPRESSO[33] suite of electronic-structure codes, was used to perform structural optimizations of a series of energetic molecular crystals at both ambient pressure and under hydrostatic compression conditions. The PWscf code allows evaluation of the total energy of periodically repeating geometries using a plane-wave basis set within the pseudopotential approximation. Following the Barone et al.[31] implementation, in the case of DFT-D calculations the total energy of the system can be expressed as

$$E_{\text{DFT-D}} = E_{\text{DFT}} + E_{\text{disp}} \tag{1}$$

where E_{DFT} is the self-consistent Kohn−Sham energy and E_{disp} is the dispersion energy term

$$E_{\text{disp}} = -\frac{1}{2}\sum_{ij} C_6^{ij}\left[\sum_{\vec{R}} |\vec{r}_{ij} + \vec{R}|^{-6}\, f_{\text{damp}}(|\vec{r}_{ij} + \vec{R}|)\right] \tag{2}$$

In eq 2 $\vec{r}_{ij}$ is the interatomic vector distance, $\vec{R} = l\vec{a} + m\vec{b} + n\vec{c}$ are the lattice vectors with l, m, and n integer numbers, and f_{damp} is the damping function defined as

$$f_{\text{damp}}(|\vec{r}_{ij} + \vec{R}|) = s_6\left\{1 + \exp\left[-d\left(\frac{|\vec{r}_{ij} + \vec{R}|}{r_{0,ij}} - 1\right)\right]\right\}^{-1} \tag{3}$$

TABLE 1: Comparison of the Crystallographic Parameters Calculated[a] Using DFT-D Method and the Corresponding Experimental Values

	crystal	space gr	Z	a (Å)	b (Å)	c (Å)	α (deg)	β (deg)	γ (deg)	Vol (Å^3)
1.	α-RDX[37]	*Pbca*	8	13.182	11.574	10.709	90.0	90.0	90.0	1633.86
	(CTMTNA)	(295 K)		13.237 (0.42)	11.391 (−1.58)	10.770 (0.57)	90.0	90.0	90.0	1623.94 (−0.61)
2.	β-HMX[39]	$P2_1/n$	2	6.5209	10.7610	7.3062	90.0	102.058	90.0	501.37
		(20 K)		6.544 (0.36)	10.829 (0.64)	7.391 (1.17)	90.0	102.67 (0.60)	90.0	511.11 (1.94)
	β-HMX[40,41]	$P2_1/c$	2	6.533	11.030	8.699	90.0	124.45	90.0	516.90
	(OCHTET12)	(295 K)		6.540 (0.11)	10.811 (−1.98)	8.742 (0.50)	90.0	124.28 (−0.14)	90.0	510.79 (−1.18)
3.	α-HMX[42]	*Fdd*2	8	15.140	23.890	5.913	90.0	90.0	90.0	2138.70
	(OCHTET)	(295 K)		15.140 (−0.00)	23.383 (−2.12)	5.890 (−0.37)	90.0	90.0	90.0	2085.52 (−2.49)
4.	δ-HMX[43]	$P6_1$	6	7.711	7.7110	32.553	90.0	90.0	120.0	1676.27
	(OCHTET03)	(295 K)		7.595 (−1.51)	7.595 (−1.51)	32.969 (1.28)	90.0	90.0	120.0	1648.88 (−1.75)
5.	ε-HNIW[45]	$P2_1/n$	4	8.791	12.481	13.285	90.0	106.55	90.0	1397.24
	(PUBMUU12)	(100 K)		8.916 (1.42)	12.514 (0.27)	13.413 (0.97)	90.0	106.58 (0.03)	90.0	1434.43 (2.66)
6.	β-HNIW[46]	$Pb2_1/a$	4	9.6765	13.0063	11.6493	90.0	90.0	90.0	1466.11
	(PUBMUU01)	(295 K)		9.659 (−0.18)	13.251 (1.88)	11.485 (−1.41)	90.0	90.0	90.0	1469.96 (0.26)
7.	γ-HNIW[45]	$P2_1/n$	4	13.0342	8.1773	14.7465	90.0	108.56	90.0	1489.95
	(PUBMUU07)	(100 K)		13.214 (1.38)	8.223 (0.56)	14.764 (0.12)	90.0	108.83 (0.24)	90.0	1518.58 (1.92)
8.	NM[47]	$P2_12_12_1$	4	5.1832	6.2357	8.5181	90.0	90.0	90.0	275.31
	(NTROMA13)	(4 K)		5.1654 (−0.34)	6.2825 (0.75)	8.5259 (0.09)	90.0	90.0	90.0	276.67 (0.50)
9.	DNCP[49]	$P2_1/n$	4	5.212	18.493	6.220	90.0	114.13	90.0	547.13
	(FOHMUK)	(295 K)		5.108 (−1.99)	18.215 (−1.50)	6.193 (−0.43)	90.0	114.08 (−0.05)	90.0	526.14 (−3.84)
10	TATB[50]	$P\bar{1}$	2	9.010	9.028	6.812	108.58	91.82	119.97	442.52
	(TATNBZ)	(295 K)		9.077 (0.75)	9.087 (0.65)	6.693 (−1.74)	111.82	91.56 (−0.28)	119.97	428.20 (−3.24)
11.	TNT-phase I[51]	$P2_1/a$	8	14.9113	6.0340	20.8815	90.0	110.365	90.0	1761.37
	(ZZZMUC08)	(100 K)		15.029 (0.79)	5.978 (−0.92)	20.908 (0.13)	90.0	110.81 (0.41)	90.0	1756.04 (−0.30)
12.	PNC[52]	$P2_1/c$	4	6.637	23.275	7.860	90.0	113.21	90.0	1115.91
	(NACXEU)	(295 K)		6.688 (0.78)	23.230 (−0.19)	7.805 (−0.70)	90.0	113.08 (−0.11)	89.98	1115.62 (−0.03)
13.	PETN[54]	$P\bar{4}2_1c$	2	9.2759	9.2759	6.6127	90.0	90.0	90.0	568.97
	(PERYTN12)	(100 K)		9.4007 (1.35)	9.4007 (1.35)	6.5539 (−0.89)	90.0	90.0	90.0	579.19 (1.81)
14.	FOX-7[55]	$P2_1/n$	4	6.9209	6.5515	11.2741	90.0	90.06	90.0	511.19
	(SEDTUQ02)	(200 K)		6.9873 (0.96)	6.4488 (−1.57)	11.2919 (0.16)	90.0	90.98 (1.02)	90.0	508.74 (−0.48)
15.	γ-RDX[63,64]	$Pca2_1$	8	12.6319	9.5554	11.0036	90.0	90.0	90.0	1328.17
	(RDX-d_6)	(293K) (4.78 GPa)		12.719 (0.69)	9.544 (−0.11)	10.948 (−0.50)	90.0	90.0	90.0	1329.18 (0.08)
	(RDX-h_6)	$Pca2_1$ (293K) (5.2 GPa)	8	12.5650	9.4769	10.9297	90.0	90.0	90.0	1301.47
				12.699 (1.07)	9.503 (0.28)	10.918 (−0.10)	90.0	90.0	90.0	1317.66 (1.24)

[a] The computed values correspond to the second line for each entry and were determined at a cutoff energy of 80 Ry.

For each atomic pair *ij* the dispersion coefficients $C_6^{ij} = (C_6^i C_6^j)^{1/2}$ and the sum of vdW radii $r_{0,ij} = r_{0i} + r_{0j}$ were determined using the parameters previously proposed by Grimme.[29] Following Grimme[29] we selected the functional-dependent global scaling factor parameter $s_6 = 0.75$ and the parameter $d = 20$.

In DFT calculations, the electron−ion interaction was described using ultrasoft pseudopotentials of the Vanderbilt type[34] while the generalized-gradient approximation functional of Perdew, Burke, and Ernzerhof (PBE)[35] has been used for the treatment of exchange and correlation. For each of the molecular systems of interest we investigated the convergence of crystallographic parameters for kinetic energy cutoffs ranging from 25 to 80 Ry. The use of high cutoff energies is generally required to achieve convergence of the stress tensor. The Brillouin zone sampling has been obtained using a Monkhorst−Pack[36] set of k-points with a spacing of about 0.35 Å^{-1}. The optimization of the unit cells has been done by relaxing all atoms in the cell and by minimizing the isotropic stress. The initial configuration of the system was taken to correspond to the experimental structure. The threshold criteria used in calculations were 10^{-6} Ry for the total energy, 10^{-4} Ry/bohr for the total force and 0.5 kbar for the isotropic stress of the unit cell.

3. Results and Discussions

The set of molecular materials considered in this study was selected to cover a small but representative set of compounds for energetic materials applications. In particular we have included here three of the most extensively studied nitramine systems, that is, hexahydro-1,3,5-trinitro-1,3,5-*s* triazine (RDX), 1,3,5,7-tetranitro-1,3,5,7-tetraazacyclooctane (HMX), and 2,4,6,8,10,12-hexanitrohexaazaiso-wurtzitane (HNIW) (also known as CL20), for which the crystallographic information has been obtained at both ambient and under different pressures conditions. Additionally, we extended the analysis to other types of chemical compounds, namely nitroalkane systems nitromethane and trans-1,2,-dinitrocyclopropane, hereafter denoted as NM and DNCP, the nitrocubane compound 1,2,3,5,7-pentanitrocubane, hereafter denoted as PNC, the nitrate ester compound pentaerythritol tetranitrate (PETN), nitroaromatics such as 2,4,6-trinitro-1,3,5-benzenetriamine (TATB) and 2,4,6-trinitrotoluene (TNT) and amino-nitro derivatives such as 1,1-diamino-2,2-dinitroethylene (FOX-7). For the NM, TATB and PETN crystals, experimental compression data are also available. The corresponding crystallographic information for this entire set of crystals is summarized in Table 1. Here, the aforementioned acronyms are used to describe each chemical system (and where available by the corresponding Cambridge Structural Database (CSD) reference code given in parentheses).

3.1. RDX, HMX and HNIW Nitramine Crystals. ***3.1.1. RDX Crystal.*** The first system from the series of nitramines analyzed here is RDX. For this crystal two polymorphic forms (denoted as α- and β-phases) are known to exist

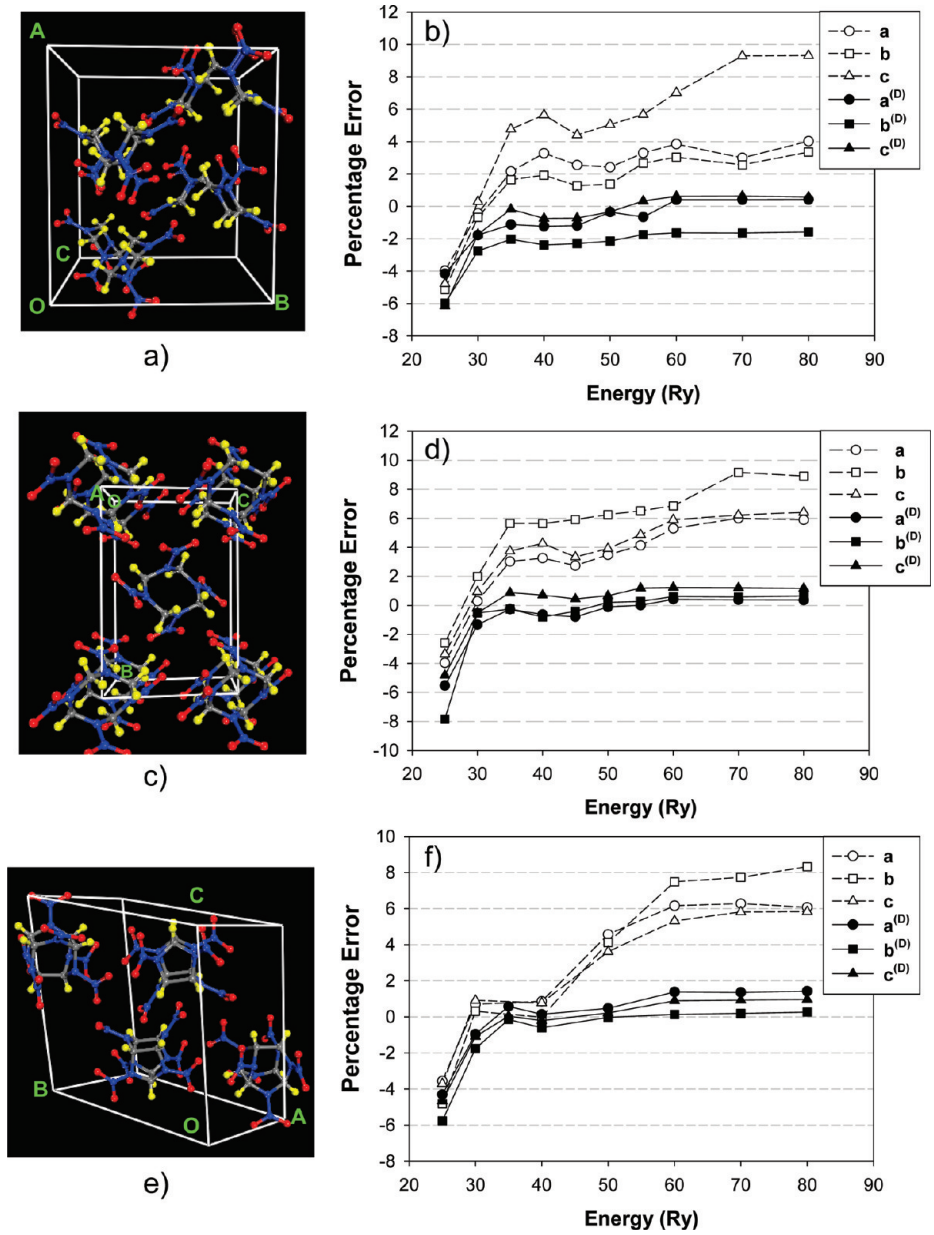

Figure 1. Pictorial view of the crystallographic unit cells for the series of nitramine crystals. (a) α-RDX, (c) β-HMX (with $P2_1/n$ symmetry) and (e) ε-HNIW. Panels (b,d,f) indicate the corresponding percentage errors of the predicted lattice parameters with cutoff energy using conventional DFT (a, b, and c) and DFT-D ($a^{(D)}$, $b^{(D)}$, and $c^{(D)}$) methods, respectively.

at ambient pressure but among these only the α-phase is stable. The crystal structure of the α-phase has been characterized by single-crystal neutron diffraction technique and the corresponding experimental lattice parameters are indicated in the first entry of Table 1.[37] The crystal structure is orthorhombic with space group *Pbca* and contains $Z = 8$ molecules per unit cell (see Figure 1a). In this phase the RDX molecule adopts a chair configuration in which two of the nitro groups occupy pseudoaxial positions while the third group adopts a pseudoequatorial position.

The bulk unit cell of the α-RDX crystal containing a total of 168 atoms (24 C, 48 N, 48 O, 48 H) has been optimized using the conventional DFT method with a $4 \times 4 \times 4$ grid of k-points and different cutoff energies ranging from 25 to 80 Ry. The results of these optimizations at various kinetic energy cutoffs are indicated with open symbols in Figure 1b) as percent errors of the predicted lattice dimensions relative to experimental values. The evolution of the calculated results indicates that important variations take place with the increase in cutoff energy. The general trend of the lattice parameters and of the corresponding errors is to increase with the cutoff energy but this increase is nonlinear with an oscillatory behavior around 40 and 70 Ry. In the region of low energies ($E_{cut} < 30$ Ry) the calculated lattice parameters underpredict the experimental values but overpredict the same data at higher cutoff energies ($E_{cut} > 30$ Ry). Overall, there is no clear convergence with the increase in cutoff energy and at the largest cutoff energy employed here of 80 Ry (1088 eV) the calculated percent errors for the *a*, *b*, and *c* lattice parameters are quite high with values of 4.0, 3.4, and 9.3%, respectively. These results clearly indicate that conventional DFT method overestimates significantly the bulk dimensions and consistent convergence of the bulk parameters is hard to obtain even for the high cutoff energies considered here. These findings are similar to those determined before by Byrd et al.[23] These authors have determined based on plane-wave DFT calculations using the PW91 and PBE

functionals that the calculated lattice dimensions significantly overestimate the experimental values, independent of the choice of exchange-correlation functional, and errors as large as 9.6% were observed for the *c* lattice dimension at a kinetic energy cutoff of 800 eV.

We turn now the attention to the case of DFT-D results. Calculations in these cases have been performed using the same k-point set and cutoff energies as for conventional DFT. The corresponding percent differences of the predicted lattice dimensions *a*, *b*, and *c* relative to experimental values are presented also in Figure 1b using dark filled symbols. In this case, the convergence trend of the predicted lattice dimensions is much better behaved, particularly for cutoff energies larger than 60 Ry. Additionally, the corresponding error bars for the calculated lattice dimensions and for the unit cell volume are significantly smaller with values of only 0.42% (*a*), −1.58% (*b*), 0.57% (*c*), and −0.61% (*V*) respectively at $E_{cut} = 80$ Ry (see also the calculated data for entry 1 in Table 1). It is clear that the large errors observed in the case of conventional DFT calculations are significantly reduced to values less than 1.58% in the case of DFT-D results.

3.1.2. HMX Crystal. The second nitramine system analyzed here is the HMX crystal. This compound can exist in four different polymorphic phases, denoted as α, β, γ, and δ, among which the stable phase at low and ambient temperatures is β-HMX. The crystal structure of the β phase is monoclinic with $Z = 2$ molecules per unit cell. Two different settings have been proposed for this phase, one with $P2_1/n$ symmetry as determined by Kohno et al.[38] and more recently by Zurova et al.[39] and a second one with $P2_1/c$ symmetry as originally identified by Choi and Boutin[40] and later by Olinger et al.[41] For completeness, in this study we have investigated both of these two settings and the corresponding experimental crystallographic parameters are indicated in entry 2 of Table 1. In the case of $P2_1/n$ setting (see data in Table 1 and in Figure 1c,d) we have selected for comparison the most recent experimental values obtained by Zurova et al.[39] at low (20 K) temperatures. The corresponding results corresponding to the crystal structure with $P2_1/c$ symmetry are presented in Figure S1 of the Supporting Information section.

The results of bulk optimization for β-HMX with $P2_1/n$ symmetry (see Figure 1d) using conventional DFT show a similar trend with the one observed for RDX. After an initial increase with cutoff energy followed by an oscillatory region, the calculated lattice parameters reach a converging plateau at high cutoff energies. Despite a somewhat better defined convergence with cutoff energy than in RDX case, the final calculated lattice parameters still overestimate the experimental data by 6.4, 5.9, and, respectively, 8.9% at $E_{cut} = 80$ Ry while the corresponding deviation of the unit cell volume is 20.1%. We note that these error levels for the lattice vectors are similar to those determined before by Byrd et al.[23] based on PW91 results.

The use of DFT-D method has a major impact upon the predicted crystallographic values (see Figure 1d). In this case the lattice dimensions reach converging values once the cutoff energy is increased beyond 55 Ry and the corresponding error bars relative to experiment are very small. Specifically, at 80 Ry the relative errors for lattice parameters are 0.36% for *a*, 0.64% for *b*, and 1.17% for *c* leading to an overall error for the unit cell volume of only 1.94%. Similar good predictions have been obtained in the case of β-HMX phase having $P2_1/c$ symmetry as illustrated in Supporting Information Figure S1. In this case, the largest deviation of the predicted lattice parameters (see data in entry 2 of Table 1) is −1.98% relative to the room temperature experimental values from ref 41 and with a small deviation of only −1.18% for the calculated unit cell volume.

An important question is if successful prediction of the β-HMX lattice parameters is limited to the low temperature phase or if accurate predictions can be obtained for other phases of this crystal. To answer this question, we have analyzed two other phases of the HMX crystal, namely the α- and δ-phases. Both these two phases exist only at high temperatures, the α phase is stable in the temperature range 103−162 °C and has an orthorhombic *Fdd2* ($Z = 8$) symmetry[42] while the δ phase is stable above 160 °C until the melting point and has a hexagonal $P6_1$ ($Z = 6$) symmetry.[43] The γ-polymorph indicated earlier in this section is a hydrate, metastable phase at ambient pressure and has not been considered here. The crystallographic information for the α and δ phases is provided in entries 3 and 4 of Table 1 together with the results of DFT-D optimizations at 80 Ry. As seen from these data both these two phases have lattice parameters close to those determined experimentally with the largest errors of −2.12 and −1.51% for the α- and δ-phases respectively and with deviations of the corresponding unit cell volumes of −2.49 and −1.75%, respectively. The slight underestimation of the unit cell volumes in both these two cases can be due to neglect of the thermal expansion effects in theoretical calculations relative to experimental data obtained at ambient temperature. Despite these small differences the results obtained clearly support the fact that DFT-D method is capable to predict accurately the crystallographic parameters of all three β-, α-, and δ-phases of the HMX crystal.

3.1.3. HNIW (CL20) Crystal. The last compound from the series of nitramines considered in this study is the polycyclic HNIW also called CL20. This system can exist in at least 5 different polymorphic phases, each of which has been resolved by X-ray diffraction.[44–46] In this study we will focus on the nonhydrate phases of HNIW, ε, β and γ, which are stable at ambient conditions. The ε-polymorph (see Figure 1e) crystallizes in the $P2_1/n$ space group,[45] the β polymorph has an orthorhombic structure with $Pb2_1/a$ symmetry[46] while the γ-HNIW has a monoclinic $P2_1/n$ symmetry.[45] In all of these cases there are $Z = 4$ molecules per unit cell. The corresponding experimental crystallographic data for these polymorphs are presented in entries 5, 6, and 7 of Table 1.

A detailed analysis of the results obtained using conventional DFT and DFT-D methods for the ε polymorph is represented in Figure 1f. For both methods the optimizations have been done using a $5 \times 4 \times 4$ grid of k-points. As in previously discussed cases, the error bars for results using the conventional DFT method remain high with a maximum deviation of 7.7% at 80 Ry for the *c* lattice parameter. In contradistinction, in the case of DFT-D method these errors are substantially reduced to values of 1.42, 0.27, and 0.97% at $E_{cut} = 80$ Ry with respect to the low-temperature data obtained by Bolotina et al.[45] Moreover, this good level of agreement with experimental data is obtained not only for the case of ε-HNIW phase but for the other two polymorphs β- and γ-HNIW. Indeed, for these two phases (see entries 6 and 7 in Table 1) the largest deviations of the lattice parameters are 1.88% (1.38%) with respect to corresponding experimental data.[45,46]

As a final note, it is interesting to compare the level of agreement obtained using our classical force field[14–16] for description of nitramine crystals to the current set of DFT-D results. As briefly indicated in Introduction, prediction of nonreactive crystallographic properties of nitramine crystals has

been done using classical pairwise atom−atom (6-exp) Buckingham potentials with inclusion of the electrostatic interactions between the atoms of different molecules. The parametrization of this force field was done to reproduce the lattice parameters and the lattice energy of α-RDX crystal and then was assumed to be transferable to other nitramine crystals. The results of molecular packing calculations using this classical force field for the lattice parameters are $a = 13.286$ Å (0.79%), $b = 11.651$ Å (0.67%), $c = 10.608$ Å (−0.94%) for α-RDX, $a = 6.475$ Å (−0.69%), $b = 10.831$ Å (0.66%), $c = 7.373$ Å (0.92%) for β-HMX, and $a = 8.857$ Å (0.76%), $b = 12.488$ Å (0.06%), $c = 13.463$ Å (1.34%) for ε-HNIW, where the values in parentheses represent the percentage error deviations with respect to experimental values indicated in Table 1. It can be clearly seen that the relative errors obtained in these cases are fully comparable to those obtained in DFT-D calculations, supporting the view that molecular crystal structure prediction can be done accurately as long as a proper description of the vdW interactions is considered.

The ensemble of the above presented results for the RDX, HMX, and HNIW nitramine crystals indicate that the DFT-D method provides significant improvements relative to conventional DFT in prediction of the bulk lattice and volume parameters. The corresponding error bars are quite small with maximum deviations of 1.6−2.1%, depending on the reference experimental set used for comparison. Moreover, for the entire set of structures investigated the predicted unit cell volumes are within 2.6% from the corresponding experimental values. Given these encouraging results we will focus in the next sections on extending our analysis to other classes of chemical compounds.

3.2. Nitroalkane Compounds: NM and DNCP Crystals. Further assessment of the performances of the DFT-D method to predict the structural properties of energetic molecular crystals was done for the nitroalkane compounds NM and DNCP. NM represents a prototypical explosive for which a broad range of properties under a wide range of conditions have been investigated. A comprehensive list of such properties can be found in our previous work.[20] Among these properties, relevant for the current work is the accurate determination of the crystalline structure of NM based on neutron powder diffraction measurements performed at 4 K.[47] At low temperatures, the NM crystal has an orthorhombic unit cell with $P2_12_12_1$ symmetry and $Z = 4$ molecules in the unit cell (see Figure 2a). The specific crystallographic information for NM is provided in entry 8 of Table 1. The availability of the NM crystal structure determined using highly accurate neutron diffraction data at a low temperature of 4.2 K where thermal contributions are negligible represents an ideal case for direct comparison with results of the DFT-D calculations.

The bulk unit cell of the NM crystal has been optimized using conventional DFT and DFT-D methods using a $6 \times 5 \times 4$ Monkhorst-Pack grid of k-points and the corresponding results are presented in Figure 2b as function of different cutoff energies. The variation of the calculated lattice parameters with the increase in cutoff energy is similar to the one observed for the nitramine crystals discussed above. Specifically, in the case of conventional DFT results, the calculated lattice parameters increase with cutoff energy leading to highly overestimated values relative to experiment. Large dispersions of the individual lattice errors are observed ranging from 2.65% for the a lattice vector to 5.81 and 10.5% for c and b lattice vectors, respectively, at $E_{cut} = 80$ Ry. A similar trend and dispersion of the predicted lattice parameters were obtained before by Byrd et al.[23] using the PW91 functional, with the largest deviation of 8.5% for the b lattice vector at a cutoff energy of 40 Ry (545 eV). These results again confirm the limited performances of conventional DFT in predicting the crystallographic structure of molecular crystals.

A very different picture emerges from the analysis of the DFT-D results. From the data in Figure 2b, it can be seen that the calculated lattice parameters reach converging values for cutoff energies above 55 Ry. At the highest cutoff energy of 80 Ry, the calculated errors for the a, b, and c lattice parameters are only −0.34, 0.75, and 0.09% relative to the neutron diffraction data[47] and with a unit cell volume deviation of only 0.50% (see also entry 8 in Table 1). This high level of agreement to accurate experimental data almost free of thermal contributions further confirm the strength of the DFT-D method. We note that similar very good predictions of the crystallographic lattice parameters of NM with errors of −0.1, 0.6, and 0.2% have been obtained recently by Conroy et al.[48] Simulations in that study were also done using an empirical vdW correction to DFT based however on the method developed by Neumann and Perrin.[11]

In the case of the DNCP crystal with monoclinic symmetry $P\bar{1}$ ($Z = 4$) (see Figure 2c) the experimental crystal structure is available only at 295 K.[49] The DFT-D calculations performed in this case using a $5 \times 6 \times 1$ k-point grid demonstrate again major improvements in the accuracy of the predicted lattice parameters relative to conventional DFT data. Specifically, the large errors of 5.25, 7.68, and 2.87% of the predicted a, b, and c lattice dimensions using conventional DFT decrease to −1.99, −1.50, and −0.43% in the case of DFT-D method. The overall underestimation observed in this last case is reasonable given the fact that thermal expansion contributions inherent in the experimental structure at 295 K have not been considered in our calculations.

3.3. Nitroaromatics Compounds: TATB and TNT Crystals. The analyses of the nitroaromatic compounds TATB and TNT offer new, even more challenging tests for the performance of the DFT-D method. In the case of the TATB crystal, additional difficulties are due to the low crystal symmetry and increased complexity of the interactions between molecules. The TATB crystal has a low triclinic symmetry of the $P\bar{1}$ type.[50] The molecules in this crystal are flat, of hexagonal shape, and each molecule is hydrogen bonded to six other molecules leading to formation of molecular sheets in the (a,b) plane (see Figure 2e). The neighbor molecular sheets are bonded by weak vdW interactions. Prediction of the crystal structure using conventional DFT (see the open symbols in Figure 2f) leads to intermolecular distances that are highly overestimated. In particular, the distance between molecular sheets running along the c axis is overestimated by values as high as 15%. In contradistinction, the use of the DFT-D method significantly decreases these errors as shown by the filled symbols in Figure 2f and in entry 10 of Table 1 to within 1.74% for the c axis and 0.75% for the a and b cell lengths at a cutoff energy of 80 Ry. This improvement in structural parameters predicted by DFT-D method versus conventional DFT is remarkable.

The TNT crystal represents another very important energetic material with a large number of civilian and military applications, due in part to its increased thermal stability to spontaneous detonation. This compound is known to crystallize in two polymorphic forms, a monoclinic and an orthorhombic form, with the most stable being the monoclinic phase. Structural characterization of TNT polymorphs has a long history but here we will consider for reference the most recent crystallographic

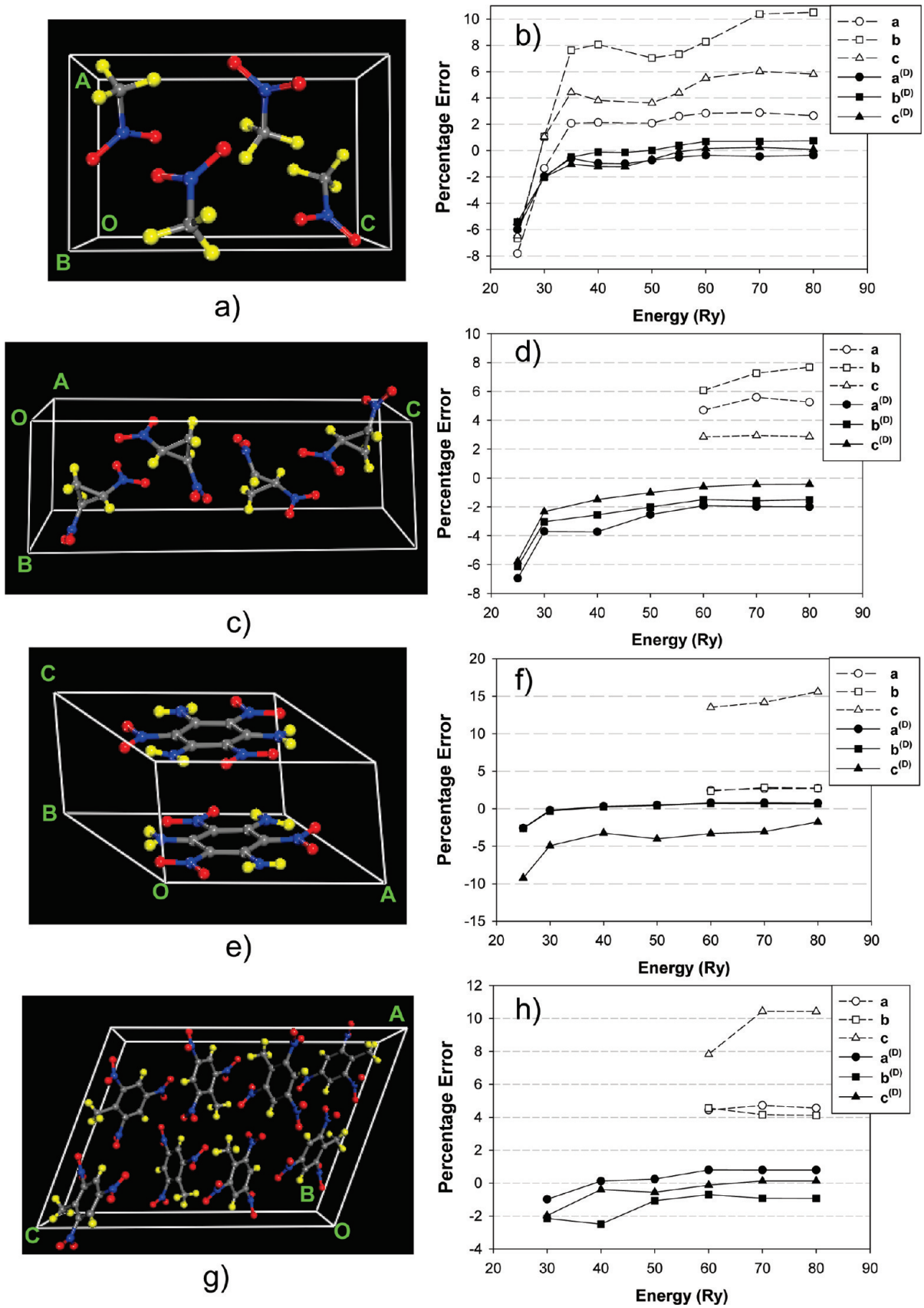

Figure 2. Pictorial view of the crystallographic unit cells for nitroalkanes (a) NM and (c) DNCP and for nitroaromatics (e) TATB and (g) TNT-I crystals. Panels (b,d,f,h) indicate the corresponding percentage errors of the predicted lattice parameters with cutoff energy using conventional DFT (a, b, and c) and DFT-D ($a^{(D)}$, $b^{(D)}$, and $c^{(D)}$) methods, respectively.

data obtained by Vrcelj et al.[51] at low temperatures (100 K). A novel crystallographic aspect of this monoclinic phase with symmetry $P2_1/a$ ($Z = 8$), hereafter denoted as TNT-(I), relative to other crystals analyzed so far in this study, is that the asymmetric part of the unit cell contains two independent molecules (denoted as A and B). The molecular arrangement

(see Figure 2g) corresponds to a layered structure along the *c* axis where each layer contains a pair of A and B molecules. The analysis of the crystallographic packing in TNT-I did not identify the existence of any hydrogen bonds and consequently it was concluded that intermolecular interactions are dominated by vdW forces.[51]

From the analysis of the lattice dimensions predicted using conventional DFT with a $2 \times 5 \times 1$ k-point grid (see Figure 2h), large deviations up to about 12% at 80 Ry are observed, particularly for the *c* direction in which the molecules are stacked in layers. This level of agreement is highly improved in the case of DFT-D method (see Figure 2h) and entry 11 in Table 1). Indeed, in this case the predicted lattice parameters reach satisfactory convergence once the cutoff energy is increased beyond 60 Ry. In this case, the corresponding error bars for the *a*, *b*, and *c* lattice vectors decrease significantly to 0.79, −0.92, and 0.13% at 80 Ry while the corresponding lattice volume differ by only −0.3% from the low temperature data obtained by Vrcelj et al.[51]

Overall the results obtained in this section for both TATB and TNT-(I) further sustain the good performances of DFT-D method for molecular crystal structure prediction.

3.4. Nitrocubanes (PNC), Nitrate Esters (PETN), and Amino-Nitro Derivatives (FOX-7) Crystals. The last group of crystals considered in our series contains selected systems from different other chemical classes, namely pentanitrocubane (PNC), pentaerythritol tetranitrate (PETN), and the amino-nitro derivative FOX-7. This selection is intended to explore new types of molecular packing motifs and chemical bonding.

The PNC compound (see Figure 3a) is one of the crystals with the highest density among various CHNO compounds, with a value of 1.96 g/cm^3 at room temperature.[52] This high density is due to a close packing in which each oxygen atom has nine nonbonded O...O contacts shorter than 3 Å. The PNC crystal adopts a monoclinic $P2_1/c$ structure with $Z = 4$ molecules per unit cell.[52] PETN represents another example of a common energetic material often used as a booster high explosive. It can exist in two polymorphic phases, a tetragonal phase PETN I (see Figure 3c) and an orthogonal PETN II phase. Among these two phases the tetragonal one with $P\bar{4}2_1c$ ($Z = 2$) symmetry is the most stable at ambient temperature and pressure conditions and is the polymorph considered in this study. In earlier studies of this crystal[53] the nature of intermolecular interactions was assigned to be of the vdW type but more recently, weak hydrogen bonds with lengths varying between 2.3 and 2.7 Å have been evidenced as well.[54] Finally, FOX-7 represents one of the more recent high density energy materials with superior shock sensitivity properties. The crystal structure as resolved based on X-ray[55] has a monoclinic $P2_1/n$ symmetry with $Z = 4$ molecules per unit cell (Figure 3e). The novelty of the chemical motif in this crystal relative to other compounds studied here is that molecular structure presents extensive π-conjugation and intramolecular hydrogen bonds between the nitro-O and the amino-H atoms. In this crystal the molecules are packed in "head-to-tail" configurations with formation of two-dimensional wave-shaped layers. Extensive hydrogen bonds are also present within these layers while weak vdW interactions exist between the layers. This type of molecular packing was found to be the key in explaining the low sensitivity to friction and impact compared to other energy materials.[56]

From the discussion above it can be seen that a wide range of intermolecular interaction types are present in the case of this set of crystals. They range from ordinary vdW interactions in highly dense CHNO crystals as is the case of PNC, to crystals with mixed vdW and weak hydrogen bonds as for PETN I, and to π-conjugated systems with extensive intra- and intermolecular hydrogen bonds within molecular layers and with weak vdW interactions between the layers. All these cases represent additional tests to evaluate the predictive capabilities of DFT-D method and to compare them to conventional DFT.

The results of DFT-D calculations for these crystals are presented in Figure 3b,d,f. In all three cases conventional DFT is highly inaccurate in prediction of the crystallographic parameters with errors as large as 8.5% for PNC, 6.15% for PETN-I, and 14.56% for FOX-7. These errors are significantly lowered in the case of DFT-D method to values of less than 0.78% for PNC, 1.35% for PETN, and −1.57% for FOX-7. This level of improvement is remarkable particularly in light of the diversity of chemical bonding between molecules in each of these crystals.

The ensemble of results presented in Sections 3.1−3.4 clearly indicate that conventional DFT method is highly inaccurate for prediction crystallographic parameters of molecular crystals due to the lack of dispersion interactions. In contradistinction, DFT-D method with dispersion coefficients as parametrized by Grimme[29] is capable of providing accurate crystallographic parameters. For the set of nitramines, nitroalkanes, nitroaromatics, nitrocubanes, nitrate esters, and amino-nitro derivatives analyzed here the overall accuracy of the calculated lattice parameters is about 2% or less relative to the experimental data. Sizable smaller errors were determined for those structures where comparison is made with experimental crystallographic data obtained at low temperatures where thermal contributions are negligible. This is, for example, seen in the case of NM crystal where the predicted lattice dimensions are within 0.75% from the neutron diffraction data measured at 4 K.[47] Similarly, small errors were found for other crystals where low temperature crystallographic data is available for comparison like for β-HMX (1.17%), ε-HNIW (1.42%), TNT-I (−0.92%), PETN (1.35%), and FOX-7 (−1.57%).

3.5. Compression Effects. Beside the optimization of the lattice parameters at zero pressure and temperature conditions a second type of problem investigated in this study is related to modification of the lattice parameters under hydrostatic compression. Compression of energetic materials has been the subject of many previous theoretical studies but relevant for this work are the results obtained by Byrd and Rice[24] using conventional DFT method. It has been found that in the case of RDX, HMX, HNIW, TATB, and PETN crystals large differences between the predicted and the experimental values were observed at low pressures but these differences decrease with the increase in pressure. It has been concluded that only in the case of pressures larger than 6−7 GPa the theoretical values approach the corresponding experimental data. Given these obvious limitations of conventional DFT, in this study we review the problem of crystal structure prediction under hydrostatic compression conditions using DFT-D method. For this purpose we have selected from the list of 10 crystals considered earlier in this study those systems for which experimental compression data are available, namely RDX,[41] β-HMX,[41] ε-HNIW,[57] NM,[58,59] TATB,[60] and PETN[61] crystals. Calculations in this case were done using the same set of k-points as for ambient pressure calculations and a cutoff energy of 60 Ry.

3.5.1. Compression of the RDX Crystal. The linear and volume compression of the α-RDX crystal has been analyzed experimentally by Olinger et al.[41] for pressures up to 9 GPa. It has been found that at a pressure of ∼4 GPa a phase transition

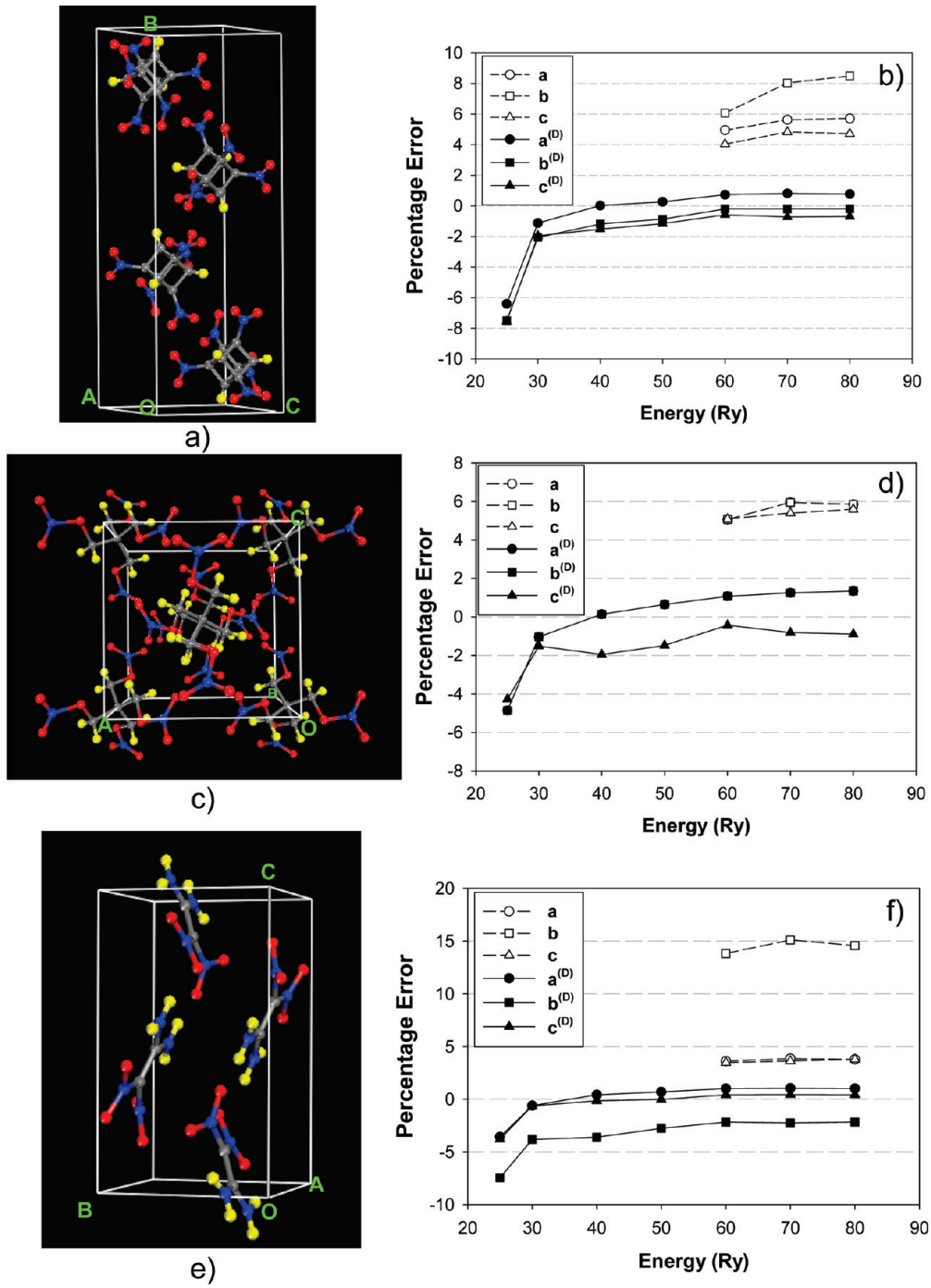

Figure 3. Pictorial view of the crystallographic unit cells for (a) nitrocubane PNC, (c) nitrate ester PETN, and (e) amino-nitro derivative FOX-7 crystals. Panels (b,d,f) indicate the corresponding variation with cutoff energy of the percentage errors of the predicted lattice parameters using conventional DFT (a, b, and c) and DFT-D ($a^{(D)}$, $b^{(D)}$, and $c^{(D)}$) methods, respectively.

$\alpha \rightarrow \gamma$ takes place with a reduction of about 1.6% in the unit cell volume. The new high pressure phase was originally assigned[41] to be orthorhombic with *Pbca* space group symmetry and $Z = 8$ molecules per unit cell. This initial assignment has received support in a study by Goto et al.[62] based on a combined use of infrared spectroscopy and powder X-ray diffraction measurements. The authors of this study have concluded that both the α and γ phases belong to the same *Pbca* space group and molecules have the same conformation. The only difference among these two phases is in the crystal packing. These findings have been put to test in a more recent study by Davidson et al.[63] Using a combination of X-ray single crystal and neutron powder diffraction it has been found that in the pressure range 3.90−7.99 GPa the RDX molecules adopt different conformations relative to the ambient phase. Moreover, the measured diffraction pattern does not support the existence of *Pbca* space group as previously stated by Goto et al.,[62] instead a different orthorhombic space group $Pca2_1$ has been assigned for the high pressure γ phase. In particular, it has been found[63] that the crystal contains two independent molecules in the asymmetric unit leading to a total of $Z = 8$ molecules in the unit cell. The results obtained by Olinger et al.[41] for α-RDX and the most recent experimental data of Davidson et al.[63] for γ-RDX have been used to tests the capabilities of DFT-D method for description of the compression properties of the RDX crystal.

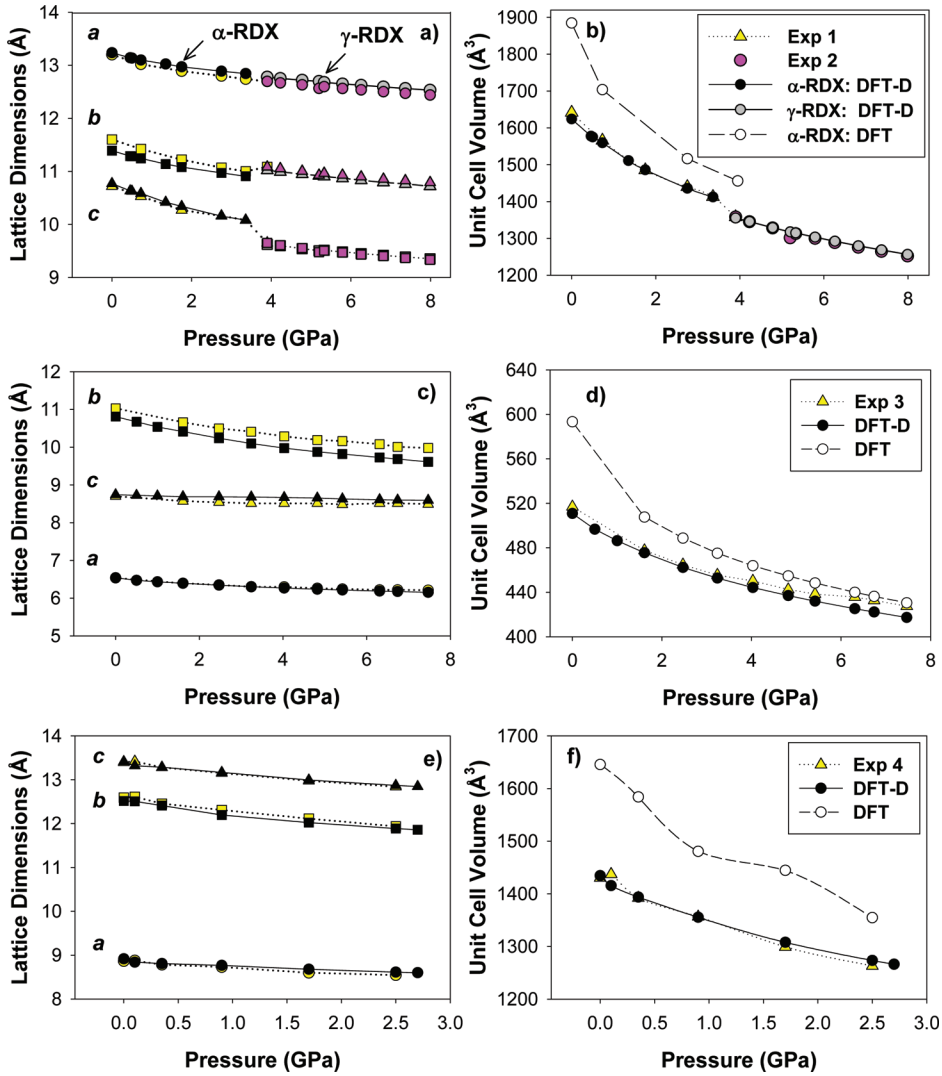

Figure 4. Variation with hydrostatic pressure of the lattice parameters and unit cell volume for (a,b) α-RDX and γ-RDX, (c,d) for β-HMX, and (e,f) for ε-HNIW as predicted using DFT-D method (dark symbols). For comparison the available experimental data from refs.[41] (Exp1) and 63 (Exp2) for α-and γ-RDX, from ref 41 (Exp3) for β-HMX, and from ref 57 (Exp.4) for ε-HNIW are indicated using yellow colored symbols while the data from ref 63 is shown using pink-filled symbols. In the case of the unit cell volume plots, the results of conventional DFT predictions from ref 24 are also included.

In this study, we have analyzed theoretically the modifications of the lattice parameters for both phases of RDX crystal in the pressure range 0−3.36 GPa for α-RDX and 3.9−7.99 GPa for γ-RDX. The corresponding lattice parameters as determined using the DFT-D method are given in Table S1 of the Supporting Information section. The corresponding variation of the calculated *(a,b,c)* lattice parameters and unit cell volume with pressure are also represented using filled black symbols in Figure 4a,b. In the same figures, we have included using yellow filled symbols the experimental data obtained by Olinger et al.[41] for α-RDX and using pink filled symbols the set of results determined by Davidson et al.[63] supplemented by data communicated by Pulham[64] for γ-RDX. Finally, in Figure 4b we also show for comparison (using open symbols) the results obtained using conventional DFT by Byrd and Rice.[24]

As can be seen from data in Figure 4a the DFT-D predicted lattice parameters for α-RDX follow very closely the corresponding experimental data. The largest difference of −1.8% is seen at ambient pressure relative to the room temperature experimental results obtained by Olinger et al.[41] (see data in Supporting Information Table S1). Upon increasing pressure, the deviation between the calculated and experimental parameters decreases continuously such that at 3.36 GPa the largest percentage error deviation is only −0.85%. Similarly, the largest difference for the calculated volumes at different pressures relative to data in ref 41 is only −1.07% and this takes place at zero pressure conditions. In contradistinction, the conventional DFT method[24] (see Figure 4b) predicts significantly larger unit cell volumes with error bars as large as 14.8% at zero pressure. These errors decrease with pressure increase but even at 3.95 GPa they remain substantial, that is, 4.8%. These results clearly indicate that DFT-D method is capable to bring substantial corrections to conventional DFT results.

Following the experimental findings obtained by Davidson et al.,[63] in the case of γ-RDX we have optimized the crystal structure using the proposed $Pca2_1$ structure over the pressure range 3.9−7.99 GPa. In Table 1, we have selected for comparison two representative sets of data at 4.78 and 5.2 GPa determined by Davidson et al.[63] using deuterated and hydrogenated RDX samples. The full set of calculated values at different pressures is given in Supporting Information Table S1 and the corresponding data points are indicated with gray filled symbols in Figure 4a,b. From this figure, it can be seen that for the entire range of pressures investigated the agreement of the calculated

data to experimental values is remarkably good. The maximum unit cell lattice deviation is only 0.75% relative to experimental values obtained for the deuterated RDX-d_6 crystal. A slightly larger difference is observed at 5.2 GPa for the case of data obtained for the nondeuterated RDX-h_6 crystal.[63] Nevertheless, even in this case the calculated DFT-D lattice parameters of a = 12.699 Å, b = 9.503 Å, and c = 10.918 Å differ by only 1.07, 0.28, and −0.10% from the results obtained by Davidson et al.[63] Practically, as can be observed from the graphs in Figure 4a,b several of the calculated values are actually superimposed on the corresponding data obtained by Davidson et al.[63,64] The calculated variations of the unit cell volumes with pressure can be fitted with a third order Birch−Murnaghan equation of state for both the α- and γ-RDX phases. The corresponding fit parameters are V_0 = 1625.56 Å^3, B_0 = 13.99 GPa and B' = 7.80 for the α-RDX and V_0 = 1555.04 Å^3, B_0 = 16.72 GPa, and B' = 8.03 GPa for γ-RDX, respectively. The calculated bulk moduli B_0 compare well to the experimental values of 13.9 GPa.[65] for α-RDX, respectively to 17.6 GPa[63,64] for γ-RDX.

Summarizing, the results obtained in this section demonstrate that over the entire set of pressures 0−3.36 GPa and 3.9−7.99 GPa considered here, the DFT-D method is capable to provide an accurate description of the pressure induced structural modifications of the α and γ phases of RDX.

3.5.2. Compression of the β-HMX Crystal. Investigation of the structural modifications of β-HMX crystal under hydrostatic compression conditions has been performed by Olinger et al.[41] in the pressure range 0−7.47 GPa. The crystal was found to remain stable and maintains its monoclinic structure described by $P2_1/c$ space group over the entire pressure range. As indicated in Section 3.1.2 two different settings $P2_1/c$ and $P2_1/n$ have been proposed for this crystal and for completeness in this study we analyzed the compression data for both these two cases. The calculated results are given in Supporting Information Tables S2 and S3. Here we limit our discussion to the case of the crystal with $P2_1/c$ symmetry to facilitate comparison to experimental data.[41]

In Figure 4c,d, we compare the experimental crystallographic values (represented using yellow filled symbols) obtained by Olinger et al.[41] with the DFT-D predictions (represented using black filled symbols). The overall agreement for the lattice dimensions is reasonably good. For the a and c lattice parameters the maximum difference between calculated and experimental values remain relatively small with deviations less than 2.0%. However, in the case of the b lattice vector the error bars are larger, ranging from −1.98% at ambient pressure to −3.6% at the highest pressure of 7.4 GPa. This increased deviation at larger pressures is also noticeable in the variation of the unit cell volume (see Figure 4d) where theoretical values systematically under-predict the experimental results. Among various crystals analyzed in this study the magnitude of these differences between experimental and theoretical results is the highest. The reason for these differences is not easily evidenced. One potential reason can be due to the lack of thermal effects in theoretical predictions leading to an overall underestimation of the crystallographic parameters. The magnitude of such thermal contributions can be obtained for example in the case of the β-HMX crystal structure resolved within $P2_1/n$ symmetry by comparing the low temperature (20 K) values obtained by Zhurova et al.[39] with the room temperature data obtained by Kohno et al.[38] The corresponding changes were found to be about −2.44% for lattice parameters and −3.05% for the unit cell volume, practically the same order of magnitude as the calculated differences between theoretical and experimental results identified above.

In Figure 4d, beside the DFT-D results we also indicate the results of standard DFT calculations from ref 24. In this case, the unit cell volume is overestimated by values as large as 14.6% at low pressure but the agreement with experimental data is improved as the pressure increases such that at 7.4 GPa a deviation of only 0.75% is observed.

3.5.3. Compression of ε-HNIW Crystal. The results of bulk optimization for ε-HNIW phase at different pressures using DFT-D method are indicated in Figure 4e,f and the corresponding crystallographic parameters are given in Supporting Information Table S4. In these figures theoretical results are compared with experimental data of Pinkerton.[57] Overall the predicted lattice parameters were found to be very close to experimental values over the entire pressure region investigated. As seen from the data in Supporting Information Table S4 the largest deviations between theoretical and experimental data remain below 0.91% (1.51%) for lattice dimensions and respectively for the unit cell volume. In contradistinction, the standard DFT results from ref 24 indicate (see Figure 4f) substantial larger errors ranging from 15.6% at zero pressure to 7.3% at 2.5 GPa.

Overall, the ensemble of results presented above support the fact that DFT-D method is capable to describe accurately the compression data for RDX, HMX, and HNIW crystals, including the high pressure γ-RDX phase as resolved by Davidson et al.[63]

3.5.4. Compression Results for NM, TATB, and PETN Crystals. Beside the class of nitramine crystals it is also important to determine if the accuracy of the DFT-D method to predict hydrostatic compression effects can be extended to other classes of chemical compounds. This problem is analyzed in the current section for the case of non-nitramine systems NM, TATB, and PETN. As mentioned before our specific selection is motivated by the availability of the experimental data necessary to facilitate validation of the corresponding theoretical results.

In the case of NM crystal, two sets of experimental values have been selected for comparison. The first one corresponds to single crystal X-ray results obtained by Cromer et al.[58] in the pressure range 0.3 to 6.0 GPa while the second set is represented by the recent results obtained by Citroni et al.[59] using angle dispersion X-ray diffraction experiments on NM single crystals and powder. Both these two groups have found that NM crystal structure remains orthorhombic with space group $P2_12_12_1$ over the entire range of pressures investigated.

The results of these two experimental studies, represented using yellow- and green-filled symbols, respectively, together with our DFT-D theoretical predictions of the lattice parameters and unit cell volume of NM, represented using black-filled symbols, are indicated in Figure 5a,b. The entire set of theoretical values obtained at different pressures in the range 0−7.6 GPa is provided in Supporting Information Table S5. Both from the comparison given in this table or from the visual inspection of the data in Figure 5a,b, it can be seen that a close agreement exists between theoretical and experimental sets of data and this level of agreement is improved with pressure increase. The largest deviations are observed in the case of c lattice parameter at low and intermediate pressures (0.6−3.5 GPa). In this pressure region, the experimental results have shown that the methyl group is either a freely rotator at pressures below 0.6 GPa or a hindered rotator for intermediate pressures below 3.5 GPa. These dynamic (thermal) effects are obviously not considered in our simple bulk optimizations and therefore

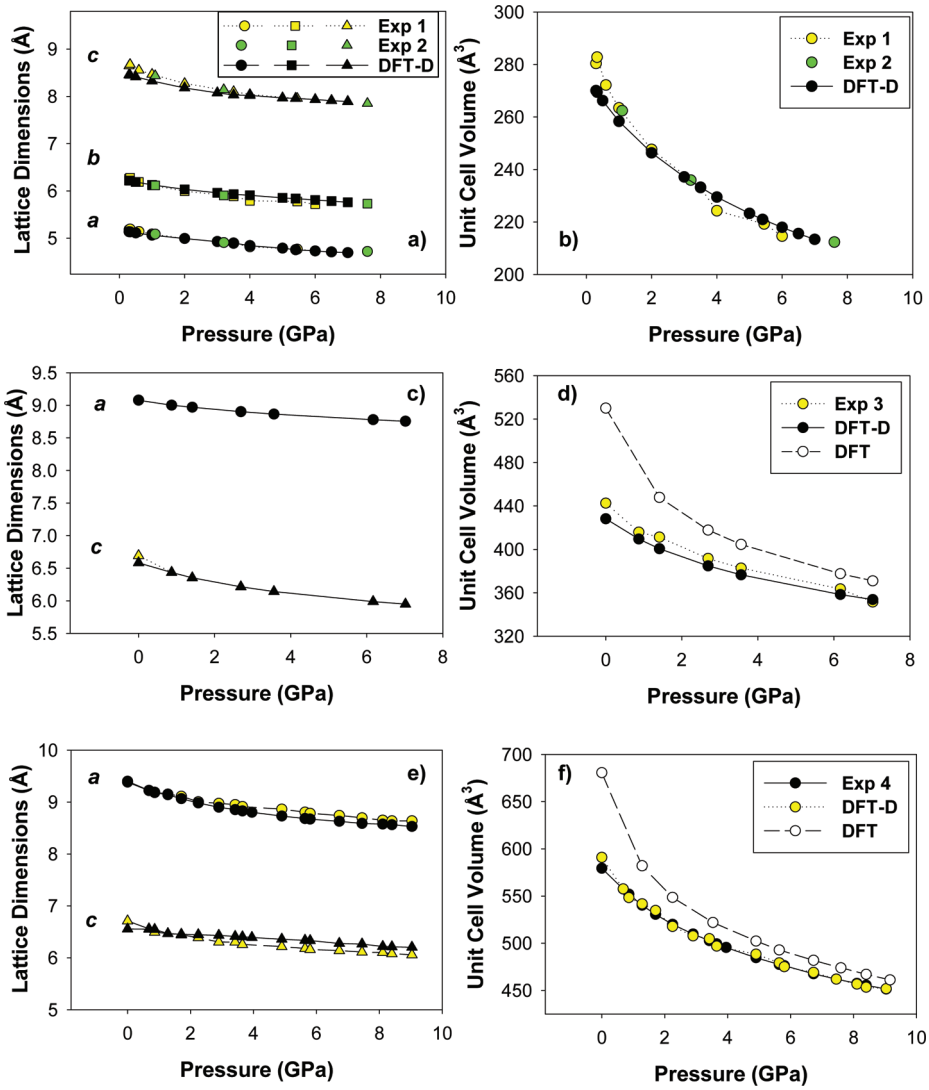

Figure 5. Variation of the lattice parameters and unit cell volume for (a,b) NM, (c,d) TATB and (e,f) PETN with pressure as predicted using DFT-D method (dark symbols). For comparison the available experimental data from ref 47 (Exp1) (yellow symbols) and ref 59 (Exp2) (green symbols) for NM, from ref 60 for TATB (yellow symbols), and from ref 61 for PETN (yellow symbols) are also indicated. In the case of the unit cell volume plots the results of conventional DFT predictions from ref 24 are also included.

they can be responsible for the slight differences between the calculated and experimental results. Once the pressure is increased beyond 3.5 GPa an almost perfect agreement is found between theoretical and experimental results. For example at 6.0 GPa the predicted *a*, *b*, and *c* lattice parameters deviate by only −0.02%, 1.53% from the corresponding experimental values of Cromer et al.[58] while at 7.6 GPa the deviations relative to Citroni et al.[59] data are practically negligible with values of −0.77, 0.08, and 0.04%, respectively.

A similar good agreement is observed for the case of the TATB crystal as indicated in Figure 5c,d and in Supporting Information Table S6 where theoretical values are compared with experimental data obtained by Olinger and Cady.[60] The largest deviations for the lattice parameters and unit cell volume are −1.74 and −3.21%, respectively, observed at zero pressure. As pressure increases, the agreement of the theoretical and experimental data improves continuously such that at the highest pressure of 7.02 GPa the maximum lattice deviation is only 0.92% and the corresponding volume error is 0.64%. In contradistinction, the error bars from conventional DFT results[24] remain quite high, ranging from 19.9% at zero pressure to 5.6% at 7.02 GPa.

The final set of data analyzed here corresponds to compression of PETN crystal. In this case, we present in Figure 5e,f our DFT-D results together with experimental values obtained by Olinger et al.[61] A full list of calculated lattice parameters is given in Supporting Information Table S7. Because of the tetragonal nature of the PETN crystal with $P\bar{4}2_1c$ group symmetry only the values for the *a* and *c* lattice parameters are indicated in Figure 5e. From Figure 5e, it can be seen that calculated crystallographic parameters follow closely the corresponding experimental values[61] over the entire pressure range but opposite trends were found for the *a* (*b*) and respectively for *c* lattice parameters at high pressures. Specifically, the lattice dimensions *a* and *b* slightly underpredicted experimental values with deviations of −1.24% at 9.04 GPa while the *c* lattice vector is overpredicted by 2.44% at the same pressure. These two opposite trends practically compensate each other such that the deviations of the unit cell volume remain smaller than 0.75% over the entire 0.68−9.4 GPa pressure range (see also the data in Supporting Information Table S7). We note that the error bars at zero pressure indicated in Supporting Information Table S7 for the predicted unit cell parameters and volume are different from those of entry 13 in Table 1 due to the fact that in the

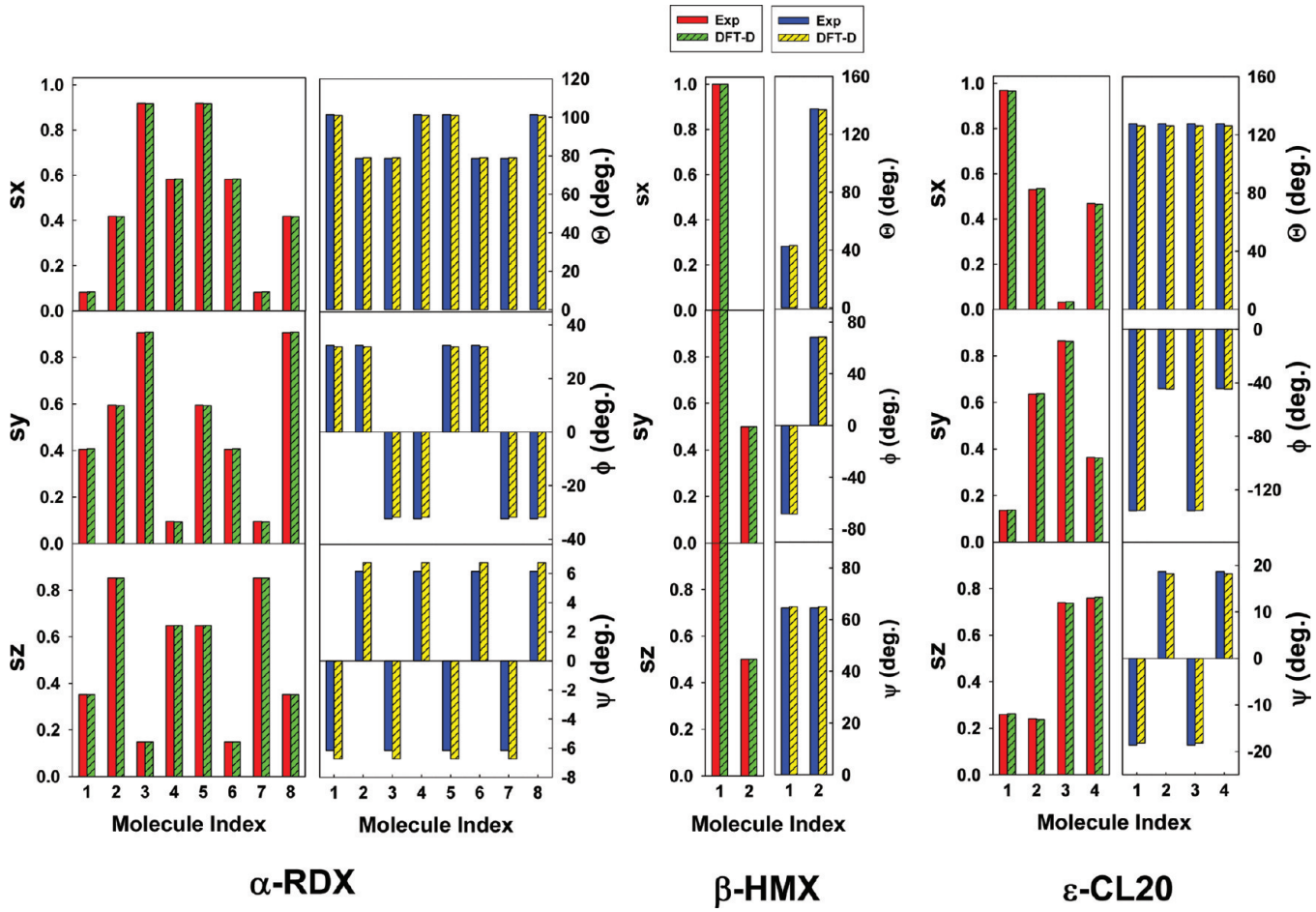

Figure 6. Comparison of the calculated center-of-mass fractional positions (*sx*, *sy*, *sz*) and Euler angles (Θ, Φ, Ψ) with experiment for each molecule in the crystallographic unit cell for α-RDX, *β*-HMX, and *ε*-HNIW crystals. Red- and green-colored bars indicate the experimental and respectively the theoretical predicted fractional positions while for Euler angles blue and yellow filled bars have been used.

former case comparison was done with data obtained at room temperature[61] while in the latest case the same comparison involved experimental data obtained at 100 K.[54] The predictions of conventional DFT method[24] over the same pressure range present significantly larger deviations ranging from 15.1% at zero pressure to 2.4% at 9.16 GPa.

On the basis of the analysis of the results presented in this and in the previous sections it can be concluded that DFT-D method with dispersion coefficients as parametrized by Grimme[29] is capable to describe accurately the modifications of crystallographic parameters under hydrostatic compression conditions. Very good agreements were found for example in the case of α-RDX (1.8%), *γ*-RDX (1.0%), *ε*-HNIW (0.9%), TATB-(1.7%) crystals where the values in parentheses indicate the maximum deviations of the lattice parameters from the experimental results over the entire range of pressures considered. The largest deviations were observed for *β*-HMX (3.67%). In the case of NM, larger errors were found in the regime of low pressures where dynamical effects such as the free or hindered rotations of the methyl groups were not considered in our static optimizations. By the increase in pressure above 3.5 GPa the level of agreement to experimental data is continuously improved with maximum deviations of only 0.77% at 7.6 GPa. Overall, these results further support the fact that DFT-D method provides significant improvements relative to conventional DFT for predicting intermolecular interactions in molecular crystals and is capable to correct the substantial overestimations of the bulk lattice parameters and unit cell volumes present in the later method.

3.6. Structural Analysis. Beside direct comparison of the predicted lattice parameters to experimental values we have also performed a comprehensive analysis of the structural content of each crystal of interest by analyzing the positions and orientations of the molecules in the unit cell. This information has been obtained by calculation of the fractional coordinates (*sx*, *sy*, *sz*) of the molecular mass centers and the corresponding Euler angles (*θ*, Φ, Ψ) for all molecules in the unit cell. This data is presented in Supporting Information Tables S8−S27 for each crystal considered in this study. In a number of instances, we have analyzed structures optimized from different sets of experimental values measured by different groups or different crystallographic settings for a given space group. Additionally, beside the orientation parameters we include in Supporting Information tables for all systems studied the root-mean-square (rms) and the maximum deviations of the predicted atomic displacements from the experimental positions for each of the symmetry-equivalent moieties. In each case, for the purpose of comparison, the mass centers of the predicted and experimental cells were located at the origin. We note that in the case of α-HMX and PETN crystals the positional and orientational information are given for each asymmetric part of the unit cell which correspond to half of an α-HMX molecule and one-fourth of a PETN molecule, respectively.

An illustrative comparison of the structural and orientational parameters to experimental data is provided in Figure 6 for the case of the α-RDX, *β*-HMX, and *ε*-HNIW crystals. From the analysis of the data in this figure it is evident that there is very little difference between the center-of-mass positions of the molecules in the predicted unit cells relative to the experimental values. Similarly, the differences in the Euler angles of the

predicted molecular structures relative to experimental data are also very small with deviations less than 0.62° for α-RDX, 0.69° for β-HMX, and 1.4° for ε-HNIW. These results confirm the fact that translational and rotational properties of the molecular systems predicted by theoretical calculations are very similar to those observed experimentally. These findings were also observed to be valid for other crystals analyzed in this work. Indeed, as indicated in Supporting Information Tables S14−S27, a very good agreement in all structural parameters between the experimental and predicted values is observed with the exception of an apparent larger deviation of the Euler angles for TATB. As discussed in earlier work by Byrd and Rice,[24] a similar result was observed in comparing conventional DFT predictions with experiment. In that work, it was found a large difference between the theoretical and experimental values of the Euler angles, but graphical depictions of superimposed unit cells showed little difference in the molecular orientations. This was attributed to the near-planarity of the molecule, in which one of the inertial axes lies along the C_3 rotational axis that is perpendicular to the plane of the molecule, and the remaining two inertial axes lie within the plane of the molecule. As explained in the previous work,[24] the Euler angles for each molecule in the TATB crystal will be dependent on the directions of these two axes within the molecular plane; however, the directions of these two inertial axes will not affect the overall molecular orientation within the unit cell. To illustrate this point we have provided a figure in Supporting Information Table S20 depicting the superimposed calculated and experimental unit cells in this case.

The ensemble of the results presented in this section further supports the fact that DFT-D method is capable to predict accurately not only the lattice parameters and the unit cell volumes but also the relative positions and orientations of the molecules in their respective crystallographic unit cell.

As a final comment, the above presented DFT-D results further expand our original studies related to the use of classical Buckingham (exp-6) intermolecular potentials for prediction the molecular packing properties of energetic molecular crystals.[14−21] Similar to classical potentials, the inclusion of potential terms proportional to C_6/R^6 for description dispersion interactions, in addition to repulsive potential terms at small atomic separations, proves to be essential in both cases to achieve accurate crystallographic predictions. The DFT-D method, however, eliminates the need for additional potential parametrization, for example, for crystals with extensive hydrogen bonding or for evaluation of specific sets of point charges and higher electrostatic multipoles for each molecular crystal of interest. Such an advantage of the DFT-D method relative to classical simulations is particularly important in compression studies of molecular crystals as charge redistribution effects and large molecular deformations at increasing pressures are difficult to model using classical potentials.

4. Conclusions

In this study we have analyzed the predictions of the dispersion-corrected DFT (DFT-D) method with the parametrization proposed by Grimme[29] for a set of 10 molecular crystals representative for energetic materials applications. This series includes molecular systems ranging from nitramines (RDX, HMX, HNIW), nitroalkanes (NM and DNCP), nitrocubanes (PNC), nitrate esters (PETN) to nitroaromatics (TATB and TNT), and amino-nitro-derivatives (FOX-7). We have also included in our analysis different polymorphic phases such as the β-, α-, and δ-phases for HMX, the ε-, β-, and γ- phases for HNIW observed experimentally at different temperatures, or the α- and γ- phases of RDX existent at different pressures.

On the basis of DFT-D calculations performed using the PBE exchange-correlation functional and ultrasoft pseudopotentials, it has been shown that crystallographic lattice parameters can be predicted with an accuracy of about 2% or less relative to the corresponding experimental data with agreement improving when the comparison is made with crystallographic data obtained at low temperatures. This is the case of systems such as NM ($\Delta = 0.75\%$, $T = 4.2$ K), β-HMX ($\Delta = 1.17\%$, $T = 20$ K), ε-HNIW ($\Delta = 1.42\%$, $T = 100$ K), TNT-I ($\Delta = -0.92\%$, $T = 100$ K), PETN ($\Delta = 1.35\%$, $T = 100$ K) and FOX-7 ($\Delta = -1.57\%$, $T = 200$ K) where the maximum percentage deviation of the lattice parameters relative to experimental data is indicated in parentheses together with the corresponding temperature where experimental data has been collected.

Beside the ambient pressure conditions, we have also investigated the hydrostatic compressions of the α-RDX, γ-RDX, β-HMX, ε-HNIW, NM, TATB, and PETN crystals over a wide variety of pressure conditions selected to match the available experimental data. It has been found that DFT-D method is capable to predict very closely both the variation of the lattice dimensions and of the unit cell volume as a result of hydrostatic compression. The corresponding maximum errors for lattice parameters over the entire range of pressures investigated were 1.8% (α-RDX), 1.07% (γ-RDX), 3.67% (β-HMX), 0.91% (ε-HNIW), 2.62% (NM), 1.74% (TATB), and 2.79% (PETN), respectively, relative to compression data obtained at ambient temperature. No experimental compression data at low temperatures were available for comparison. In the case of RDX crystal where an α→γ pressure induced phase transition takes place our calculations predict crystallographic compression data and a bulk modulus in extremely good agreement with experimental data of Davidson et al.[63,64] Finally, our analysis of the structural parameters show that DFT-D method is capable to predict not only the crystallographic parameters but also the relative positions and orientations of the molecules for the entire set of crystals considered in this study.

The above sets of results obtained at both ambient pressure or under hydrostatic compression conditions present substantial improvements relative to the conventional DFT method. Regarding the latter method, the results of both this and previous studies[23,24,48] evidenced large differences between the predicted and the experimental results ranging anywhere between 5−15%, particularly at low pressures. Only in the high pressure regime above 6 GPa, the predicted DFT values approach the corresponding experimental results.

The overall good agreement obtained between theoretical and experimental data indicate that the DFT-D method is capable to provide an adequate description of the van der Waals forces that exist in the molecular crystals analyzed here. These are welcome results given the relative simplicity of the functional form considered (see eqs 1−3) for implementation of the dispersion corrections to conventional density functionals.

Acknowledgment. We gratefully acknowledge a grant of computer time provided under DOD High Performance Computing Program at various Major Shared Resource Center Sites and discussions with Dr. Daniel Forrer of Università di Padova. The authors thank Dr. Richard Gilardi with Naval Research Laboratory, Washington, DC, Dr. Alan Pinkerton, The University of Toledo, and Dr. Colin R. Pulhman, The University of Edinburgh, U.K. for helpful discussions and for providing us experimental data prior to publication.

Supporting Information Available: Variation of the predicted lattice parameters for β-HMX (OCHTET12) ($P2_1/c$) crystal with cutoff energy using DFT-D and conventional DFT

methods are given in Figure S1. Comparison of the DFT-D predicted crystallographic parameters for α-RDX, γ-RDX, β-HMX, ε-HNIW, NM, TATB and PETN under different compression conditions with corresponding experimental data is provided in Tables S1−S7. Comparison of the molecular center-of-mass fractional positions and Euler angles for the entire set of crystals analyzed in this study are given in Tables S8−S27. This material is available free of charge via the Internet at http://pubs.acs.org.

References and Notes

(1) Kamlet, M. J.; Jacobs, S. J. *J. Chem. Phys.* **1968**, *48*, 23.

(2) Wescott, B. L.; Stewart, D. S.; Davis, W. C. *J. Appl. Phys.* **2005**, *98*, 053514.

(3) Holden, J. R.; Du, Z. Y.; Ammon, H. L. *J. Comput. Chem.* **1993**, *14*, 422.

(4) Desiraju, G. R. *Nat. Mater.* **2002**, *1*, 77.

(5) Pertsin, A. J.; Kitaigorodsky, A. In *I. The Atom-Atom Potential Method, Applications to Organic Molecular Solids*; Springer-Verlag: Berlin, 1987.

(6) Lommerse, J. P. M.; Motherwell, W. D. S.; Ammon, H. L.; Dunitz, J. D.; Gavezzotti, A.; Hofmann, D. W. M.; Leusen, F. J. J.; Mooij, W. T. M.; Price, S. L.; Schweizer, B.; Schmidt, M. U.; van Eijck, B. P.; Verwer, P.; Williams, D. E. *Acta Crystallogr. B* **2000**, *56*, 697.

(7) Motherwell, W. D. S.; Ammon, H. L.; Dunitz, J. D.; Dzyabchenko, A.; Erk, P.; Gavezzotti, A.; Hofmann, D. W. M.; Leusen, F. J. J.; Lommerse, J. P. M.; Mooij, W. T. M.; Price, S. L.; Scheraga, H.; Schweizer, B.; Schmidt, M. U.; van Eijck, B. P.; Verwer, P.; Williams, D. E. *Acta Crystallogr. B* **2002**, *58*, 647.

(8) Day, G. M.; Motherwell, W. D. S.; Ammon, H. L.; Boerrigter, S. X. M.; Della Valle, R. G.; Venuti, E.; Dzyabchenko, A.; Dunitz, J. D.; Schweizer, B.; van Eijck, B. P.; Erk, P.; Facelli, J. C.; Bazterra, V. E.; Ferraro, M. B.; Hofmann, D. W. M.; Leusen, F. J. J.; Liang, C.; Pantelides, C. C.; Karamertzanis, P. G.; Price, S. L.; Lewis, T. C.; Nowell, H.; Torrisi, A.; Scheraga, H. A.; Arnautova, Y. A.; Schmidt, M. U.; Verwer, P. *Acta Crystallogr. B* **2005**, *61*, 511.

(9) van Eijck, B. P. *J. Comput. Chem.* **2001**, *22*, 816.

(10) Day, G. M.; Cooper, T. G.; Cruz-Cabeza, A. J.; Hejczyk, K. E.; Ammon, H. L.; Boerrigter, S. X. M.; Tan, J. S.; Della Valle, R. G.; Venuti, E.; Jose, J.; Gadre, S. R.; Desiraju, G. R.; Thakur, T. S.; van Eijck, B. P.; Facelli, J. C.; Bazterra, V. E.; Ferraro, M. B.; Hofmann, D. W. M.; Neumann, M. A.; Leusen, F. J. J.; Kendrick, J.; Price, S. L.; Misquitta, A. J.; Karamertzanis, P. G.; Welch, G. W. A.; Scheraga, H. A.; Arnautova, Y. A.; Schmidt, M. U.; van de Streek, J.; Wolf, A. K.; Schweizer, B. *Acta Crystallogr. B* **2009**, *65*, 107.

(11) Neumann, M. A.; Perrin, M. A. *J. Phys. Chem. B* **2005**, *109*, 15531.

(12) Ammon, H. L.; Mitchell, S. *Propellants Explos., Pyrotech.* **1998**, *23*, 260.

(13) Dzyabchenko, A. V.; Pivina, T. S.; Arnautova, E. A. *J. Mol. Struct.* **1996**, *378*, 67.

(14) Sorescu, D. C.; Rice, B. M.; Thompson, D. L. *J. Phys. Chem. B* **1997**, *101*, 798.

(15) Sorescu, D. C.; Rice, B. M.; Thompson, D. L. *J. Phys. Chem. A* **1998**, *102*, 8386.

(16) Sorescu, D. C.; Rice, B. M.; Thompson, D. L. *J. Phys. Chem. B* **1998**, *102*, 6692.

(17) Sorescu, D. C.; Rice, B. M.; Thompson, D. L. *J. Phys. Chem. B* **1998**, *102*, 948.

(18) Sorescu, D. C.; Rice, B. M.; Thompson, D. L. *J. Phys. Chem. B* **1999**, *103*, 6783.

(19) Sorescu, D. C.; Rice, B. M.; Thompson, D. L. *J. Phys. Chem. A* **1999**, *103*, 989.

(20) Sorescu, D. C.; Rice, B. M.; Thompson, D. L. *J. Phys. Chem. B* **2000**, *104*, 8406.

(21) Sorescu, D. C.; Rice, B. M.; Thompson, D. L. *J. Phys. Chem. A* **2001**, *105*, 9336.

(22) Rice, B. M.; Sorescu, D. C. *J. Phys. Chem. B* **2004**, *108*, 17730.

(23) Byrd, E. F. C.; Scuseria, G. E.; Chabalowski, C. F. *J. Phys. Chem. B* **2004**, *108*, 13100.

(24) Byrd, E. F. C.; Rice, B. M. *J. Phys. Chem. C* **2007**, *111*, 2787.

(25) Dion, M.; Rydberg, H.; Schroder, E.; Langreth, D. C.; Lundqvist, B. I. *Phys. Rev. Lett.* **2004**, *92*, 246401.

(26) Langreth, D. C.; Lundqvist, B. I.; Chakarova-Kack, S. D.; Cooper, V. R.; Dion, M.; Hyldgaard, P.; Kelkkanen, A.; Kleis, J.; Kong, L. Z.; Li, S.; Moses, P. G.; Murray, E.; Puzder, A.; Rydberg, H.; Schroder, E.; Thonhauser, T. *J. Phys.: Condens. Matter* **2009**, *21*, 084203.

(27) Lin, I. C.; Coutinho-Neto, M. D.; Felsenheimer, C.; von Lilienfeld, O. A.; Tavernelli, I.; Rothlisberger, U. *Phys. Rev. B* **2007**, *75*, 205131.

(28) Tavernelli, I.; Lin, I. C.; Rothlisberger, U. *Phys. Rev. B* **2009**, *79*, 045106.

(29) Grimme, S. *J. Comput. Chem.* **2006**, *27*, 1787.

(30) Grimme, S.; Muck-Lichtenfeld, C.; Antony, J. *J. Phys. Chem. C* **2007**, *111*, 11199.

(31) Barone, V.; Casarin, M.; Forrer, D.; Pavone, M.; Sambi, M.; Vittadini, A. *J. Comput. Chem.* **2009**, *30*, 934.

(32) Civalleri, B.; Ugliengo, P.; Zicovich-Wilson, C. M.; Dovesi, R. *Z. Kristallogr.* **2009**, *224*, 241.

(33) Giannozzi, P.; Baroni, S.; Bonini, N.; Calandra, M.; Car, R.; Cavazzoni, C.; Ceresoli, D.; Chiarotti, G. L.; Cococcioni, M.; Dabo, I.; Dal Corso, A.; de Gironcoli, S.; Fabris, S.; Fratesi, G.; Gebauer, R.; Gerstmann, U.; Gougoussis, C.; Kokalj, A.; Lazzeri, M.; Martin-Samos, L.; Marzari, N.; Mauri, F.; Mazzarello, R.; Paolini, S.; Pasquarello, A.; Paulatto, L.; Sbraccia, C.; Scandolo, S.; Sclauzero, G.; Seitsonen, A. P.; Smogunov, A.; Umari, P.; Wentzcovitch, R. M. *J. Phys.: Condens. Matter* **2009**, *21*, 395502.

(34) Vanderbilt, D. *Phys. Rev. B* **1990**, 7892.

(35) Perdew, J. P.; Burke, K.; Ernzerhof, M. *Phys. Rev. Lett.* **1996**, *77*, 3865.

(36) Monkhorst, H. J.; Pack, J. D. *Phys. Rev. B* **1976**, *13*, 5188.

(37) Choi, C. S.; Prince, E. *Acta Crystallogr. B* **1972**, *28*, 2857.

(38) Kohno, Y.; Maekawa, K.; Azuma, N.; Tsuchioka, T.; Hashizume, T.; Imamura, A. *Kogyo Kayaku* **1992**, *53*, 227. in Japanese.

(39) Zhurova, E. A.; Zhurov, V. V.; Pinkerton, A. A. *J. Am. Chem. Soc.* **2007**, *129*, 13887.

(40) Choi, C. S.; Boutin, H. P. *Acta Crystallogr. B* **1970**, *26*, 1235.

(41) Olinger, B.; Roof, B.; Cady, H. H. *The linear and volume compresssion of β-HMX and RDX to 9 GPa (90 kilobar)*, Symposium International Sur Le Comportement Des Milieux Denses Sous Hautes Pressions Dynamiques, Commmissariat à l'Energie Atomique Centre d'Etudes de Vaujours, 27−31 aout, (Éditions du Commissariat à l'Énergie Atomique, Centre d'études nucléaires de Saclay), Paris, France, 1978; p 3.

(42) Cady, H. H.; Larson, A. C.; Cromer, D. T. *Acta Crystallogr.* **1963**, *16*, 617.

(43) Cobbledick, R. E.; Small, R. W. H. *Acta Crystallogr. B* **1974**, *30*, 1918.

(44) Gilardi, R. D. Private communication, 1997.

(45) Bolotina, N. B.; Hardie, M. J.; Speer, R. L.; Pinkerton, A. A. *J. Appl. Crystallogr.* **2004**, *37*, 808.

(46) Nielsen, A. T.; Chafin, A. P.; Christian, S. L.; Moore, D. W.; Nadler, M. P.; Nissan, R. A.; Vanderah, D. J.; Gilardi, R. D.; George, C. F.; Flippen-Anderson, J. L. *Tetrahedron* **1998**, *54*, 11793.

(47) Trevino, S. F.; Prince, E.; Hubbard, C. R. *J. Chem. Phys.* **1980**, *73*, 2996.

(48) Conroy, M. W.; Oleynik, I. I.; Zybin, S. V.; White, C. T. *J. Phys. Chem. A* **2009**, *113*, 3610.

(49) Wade, P. A.; Dailey, W. P.; Carroll, P. J. *J. Am. Chem. Soc.* **1987**, *109*, 5452.

(50) Cady, H. H.; Larson, A. C. *Acta Crystallogr.* **1965**, *18*, 485.

(51) Vrcelj, R. M.; Sherwood, J. N.; Kennedy, A. R.; Gallagher, H. G.; Gelbrich, T. *Cryst. Growth Des.* **2003**, *3*, 1027.

(52) Lukin, K.; Li, J. C.; Gilardi, R.; Eaton, P. E. *Angew. Chem., Int. Ed. Engl.* **1996**, *35*, 864.

(53) Booth, A. D.; Llewellyn, F. J. *J. Chem. Soc.* **1947**, 837.

(54) Zhurova, E. A.; Stash, A. I.; Tsirelson, V. G.; Zhurov, V. V.; Bartashevich, E. V.; Potemkin, V. A.; Pinkerton, A. A. *J. Am. Chem. Soc.* **2006**, *128*, 14728.

(55) Evers, J.; Klapotke, T. M.; Mayer, P.; Oehlinger, G.; Welch, J. *Inorg. Chem.* **2006**, *45*, 4996.

(56) Bemm, U.; Ostmark, H. *Acta Crystallogr. C* **1998**, *54*, 1997.

(57) Pinkerton, A. A. Private Communication, 1999.

(58) Cromer, D. T.; Ryan, R. R.; Schiferl, D. *J. Phys. Chem.* **1985**, *89*, 2315.

(59) Citroni, M.; Datchi, F.; Bini, R.; Di Vaira, M.; Pruzan, P.; Canny, B.; Schettino, V. *J. Phys. Chem. B* **2008**, *112*, 1095.

(60) Olinger, B. W.; Cady, H. H. *The Hydrostatic Compression of Explosives and Detonation Products to 10 GPa (100 kbar) and their Calculated Shock Compression: Results for PETN, TATB, CO_2 and H_2O*, Sixth Symposium on Detonation, San Diego, CA, Aug 24−27, 1976; Los Alamos LA-UR-76-1174, pp 1−9.

(61) Olinger, B.; Halleck, P. M.; Cady, H. H. *J. Chem. Phys.* **1975**, *62*, 4480.

(62) Goto, N.; Fujihisa, H.; Yamawaki, H.; Wakabayashi, K.; Nakayama, Y.; Yoshida, M.; Koshi, M. *J. Phys. Chem. B* **2006**, *110*, 23655.

(63) Davidson, A. J.; Oswald, I. D. H.; Francis, D. J.; Lennie, A. R.; Marshall, W. G.; Millar, D. I. A.; Pulham, C. R.; Warren, J. E.; Cumming, A. S. *CrystEngComm* **2008**, *10*, 162.

(64) Pulham, C. R. Private Communication, 2009.

(65) Yoo, C.-S., Cynn, H.; Howard, W. M.; Homes, N. *Equations of State of Unreacted High Explosives at High Pressures*, Proceedings of the Eleventh International Detonation Symposium, Snowmass Village, CO, August 31, 1998−September 4, 1998; p 951.

JP100379A